

Local magnetism and magnetoelectric effect in HoMnO_3 studied with muon-spin relaxation

H. J. Lewtas, T. Lancaster, P. J. Baker, S. J. Blundell, and D. Prabhakaran
Oxford University Department of Physics, Clarendon Laboratory, Parks Road, Oxford, OX1 3PU, UK

F. L. Pratt
ISIS Facility, Rutherford Appleton Laboratory, Chilton, Oxfordshire OX11 0QX, UK
(Dated: February 22, 2024)

We present the results of muon-spin relaxation (^+SR) measurements on the hexagonal manganite HoMnO_3 . Features in the temperature-dependent relaxation rate correlate with the magnetic transitions at 76 K, 38 K and 34 K. The highest temperature transition, associated with the ordering of Mn^{3+} moments has the largest effect on λ . The application of a static electric field of $E = 10^4 \text{ V m}^{-1}$ below $T = 50 \text{ K}$ causes a small reduction in λ which is suggestive of coupling between ferroelectric and magnetic domain walls in the ordered state of the material.

PACS numbers: 75.50.Ee, 76.75.+i, 75.80.+q, 75.60.-d

I. INTRODUCTION

The current resurgence of interest in multiferroic materials is driven by the possibility of controlling electrical charge using applied magnetic fields and magnetic moments by applied voltages. A number of compounds have been identified as being of interest in this respect¹, and recent discoveries of large magnetoelectric responses^{2,3,4,5,6} have reinvigorated the field^{7,8}. One such family of compounds is the hexagonal manganites, RMnO_3 ($R = \text{Ho}, \text{Er}, \text{Tm}, \text{Yb}, \text{Lu}, \text{Y}$), in which an electrical dipole moment results from a high-temperature structural transition. This arises because of a nonlinear coupling to nonpolar lattice distortions associated with the buckling of $\text{R}\{\text{O}$ planes and tilts of the MnO_6 bipyramids⁹. In particular, large magnetoelectric effects have been found in hexagonal HoMnO_3 ^{6,10,11} and further studies of this compound have ensued, motivated in part by its rich phase diagram^{10,12,13,14}. Magnetoelectric coupling occurs because superexchange interactions depend sensitively on orbital overlap, and these can be tuned with an electric field as metal cations and ligand anions move in opposite directions^{15,16}. Furthermore, the symmetry requirements of magnetoelectric coupling are stringent and the lower symmetry inside domain walls may allow magnetoelectric coupling between wall magnetization and ferroelectric polarization¹⁷.

One method to attempt to observe such coupling at a microscopic level is via muon-spin relaxation (^+SR). This technique is a sensitive probe of the spin distributions in a magnetic material and has proven particularly useful in probing frustration related effects⁸ including the case of the YMnO_3 ¹⁹. ^+SR can be combined with electric fields, particularly at pulsed sources of muons where the electric field can be switched on or off between muon pulses, allowing even small effects to be measured. Although combined electric field and ^+SR techniques have been extensively employed in the study of electronic states in semiconductors²⁰, it has only recently been ap-

plied to magnetic systems.²¹

In this paper, we describe the results of ^+SR measurements on hexagonal HoMnO_3 as a function of temperature and also applied electric field. We identify the source of the observed spin relaxation, follow this through the various magnetic transitions observed in the absence of an applied field, and show that a small, but measurable, contribution to the relaxation can be adjusted using an applied electric field, an effect we associate with the behavior at domain walls. This paper is structured as follows: in section II we review the magnetic and electric properties of hexagonal HoMnO_3 , in section III we describe the experiments and in section IV we present the results and discussion.

II. PROPERTIES OF HoMnO_3

A. Magnetic properties

The magnetic phase diagram of HoMnO_3 has been the subject of much experimental investigation owing to the existence of a large number of magnetic field-dependent phases^{3,12,22,23,24}. The magnetic system is based around triangular layers of $S = 2$ Mn^{3+} spins with Ho^{3+} spins between layers. The Mn^{3+} spins are coned by single-ion anisotropy to the a - b plane, and are magnetically frustrated due to the triangular geometry and antiferromagnetic (AFM) coupling. The Ho^{3+} spins, on the other hand, possess an Ising-like anisotropy forcing them to align parallel or antiparallel to the c -axis. The Mn^{3+} sublattice relieves its frustration via ordering in the a - b plane below $T_N = 72 \text{ K}$, where the Mn^{2+} spins adopt a 120 structure of the P6_3 type, shown inset in Fig. 1(a). As the temperature is reduced in zero applied magnetic field, several magnetic phases are realized which are distinguished by the absence or presence of Ho^{3+} ordering and the angle which the Mn^{3+} spins make to the local x direction (Fig. 1(a)). This angle differs by $\pi/2$ in

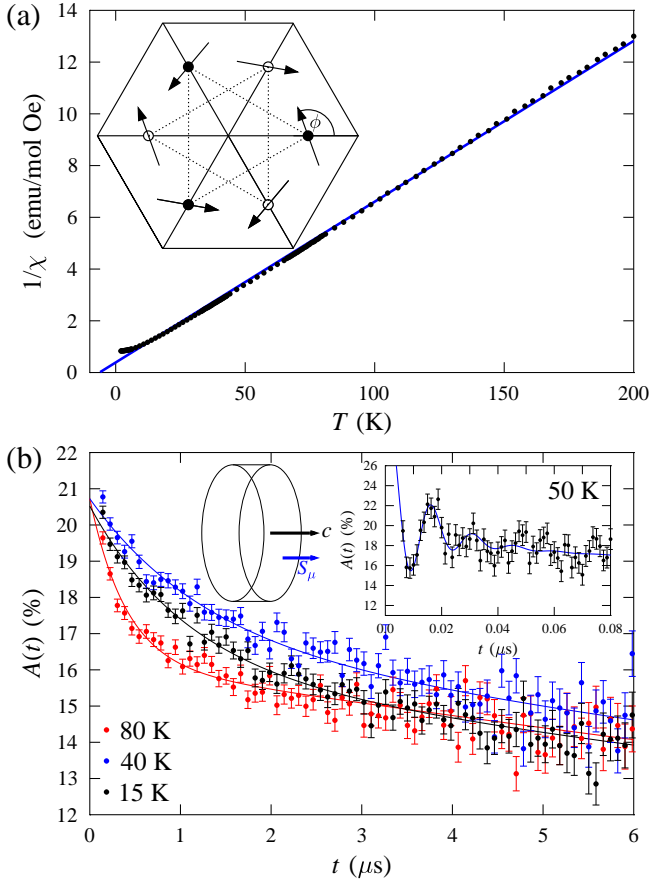


FIG. 1: (a) Evolution of the inverse field-cooled magnetic susceptibility of HoMnO_3 with temperature. Inset: magnetic order in Mn^{3+} spin system characterized by the angle ϕ . (b) ZF + SR data for HoMnO_3 measured with a pulsed muon source. The relaxation is exponential across the entire measured temperature regime. Inset, left: the experimental configuration with the initial muon spin lying parallel to the crystallographic c -axis. Filled circles represent atoms on the $z = 0$ plane, open circles in the $z = c/2$ plane. Inset, right: ZF + SR data at $T = 50$ K measured at early times using a continuous muon source. Antiferromagnetic order gives rise to the oscillations in the data.

each of the ordered phases (with the exception of a small intermediate phase described below).

The HTI phase ($P6_3cm$) occurs for $38 \text{ K} < T < T_N$ where $\phi = \frac{\pi}{2}$. In this phase the Ho^{3+} spins are disordered. Below $T = 38 \text{ K}$ the Ho^{3+} moments (at least partially) order antiferromagnetically in the c direction²⁵ while Mn spin reorientations take place. In the small temperature region $34 < T < 38 \text{ K}$ there is evidence of an intermediate magnetic phase (IP) (space group $P6_3$) characterized by an angle taking values¹⁰ $\frac{\pi}{2} < \phi < \pi$. On cooling below $T = 34 \text{ K}$, locks in to $\phi = \pi$ (the HTII phase, $P6_3cm$). Finally, a further Mn^{3+} spin rotation transition occurs around 5 K to the low temperature (LT) phase where $\phi = \frac{3\pi}{2}$ ($P6_3cm$). Here the Ho^{3+} moments also reorder to another structure, although they

are still polarized along the c -direction.

B. Electric properties

HoMnO_3 is a high T_C ferroelectric ($T_C = 875 \text{ K}$) with very large polarization of $P = 56 \text{ mCm}^{-2}$ directed along the c -axis²⁷ caused by vertical $\text{Ho}\{\text{O}$ displacements. There is also a strong magnetoelectric (ME) effect, seen as a change in electric polarization larger than $P = 80 \text{ C m}^{-2}$ in a modest magnetic field of a few tesla¹¹.

Measurements of optical second harmonic generation (SHG) and Faraday rotation suggest that the application of an electric field (E -field) of $E = 10^5 \text{ V m}^{-1}$ changes the local magnetic properties of the system considerably. At all temperatures below T_N the SHG signal is quenched in the presence of E . This was interpreted as resulting from the E -field changing the magnetic structure of the Mn^{3+} sublattice to a $\phi = 0$ arrangement and, in addition, the Ho^{3+} sublattice being forced to order ferromagnetically at all temperatures below T_N . This results in a magnetic structure described by the $P6_3cm$ spacegroup⁶. However, this picture of an E -field induced ferromagnetic Ho^{3+} sublattice contrasts with more recent magnetic x-ray results, where it was concluded that the antiferromagnetic Ho^{3+} magnetic structure remains unchanged by the application of fields $E = 10^5 \text{ V m}^{-1}$ in the region²⁵ $5 < T < 39 \text{ K}$. It has also been pointed out²⁶ that FE and AFM domain structure may be important in interpreting magnetoelectric effects in this material.

III. EXPERIMENTAL DETAILS

Samples of HoMnO_3 were prepared as described previously²⁸. Stoichiometric amount of dried Ho_2O_3 and MnO_2 powders were mixed and calcined in air for 24 hours at 1100°C and 1200°C respectively with intermediate grinding. The powders were formed into cylindrical feed rods and sintered at 1250°C for 15 hours in air. Single crystal of HoMnO_3 were grown using the coating-zone technique. The growth was carried out at a rate of 3 mm h^{-1} under the flow of mixed Ar/O_2 gas. Crystals were characterized using x-ray diffraction and dc magnetic susceptibility measurements.

In a μ^+ SR experiment, spin-polarized positive muons are stopped in a target sample, where the muon usually occupies an interstitial position in the crystal. The observed property in the experiment is the time evolution of the muon spin polarization, the behavior of which depends on the local magnetic field B at the muon site, and which is proportional to the positron asymmetry function²⁹ $A(t)$. ZF + SR measurements were made using the GPS spectrometer at the Swiss Muon Source (S μ S) and the EMU spectrometer at the ISIS facility. E -field + SR measurements were also made using the EMU spectrometer. For the measurements at S μ S an unaligned

polycrystalline sample was measured, while for the measurements at ISIS a mosaic of aligned crystals was prepared in order that the E-field could be applied along a single crystallographic direction. To produce the mosaic, HoMnO_3 crystals were polished into thin plates of thickness 1 mm with the $a\{b$ plane forming the polished surfaces. Crystallites were aligned such that the muon-spin was initially parallel to the crystallographic c -direction. Gold electrodes of thickness 1 μm were evaporated onto these surfaces allowing the application of E-fields along c . The sample were masked with insulating PTFE and mounted in an aluminium sample holder.

IV. RESULTS AND DISCUSSION

The dc magnetic susceptibility (Fig. 1(a)) shows no feature that indicates the onset of magnetic ordering at 76 K. This is consistent with previous measurements of the susceptibility³³ and is likely to be caused by the high paramagnetic susceptibility of the Ho^{3+} ions hiding the magnetic transition. No difference between the zero-field-cooled and field-cooled data is observed at low temperatures.

A. ZF + SR

Fig. 1(b) shows example ZF + SR spectra measured on HoMnO_3 . The inset shows an example spectrum measured on the unaligned polycrystalline sample at SS at $T = 50$ K. Spontaneous oscillations are seen at early times ($0 < t < 0.1$ s) in all spectra measured below T_N . Upon cooling to the HTI phase the spectra consist of oscillations at a single frequency with a large relaxation rate. In the HTII phase the oscillations change their form and there is evidence for a second frequency component. These observations are in good agreement with the results of previous + SR measurements³⁰ made on powder samples of HoMnO_3 , where oscillations were also observed below T_N .

In contrast to the measurements made at SS, those made on a single crystal using the pulsed muon source at ISIS did not show resolvable oscillations. This is because the pulse length τ_{pulse} limits the dynamic range of the measurement to rates $\Gamma = 1/\tau_{\text{pulse}}$. For muons with their initial spin direction oriented at an angle to a static magnetic field, we expect a spectrum described (in the absence of fluctuations) by

$$A(t) = A_0 \cos^2 \theta + \sin^2 \theta \cos(Bt); \quad (1)$$

where γ is the muon gyromagnetic ratio and B is the local magnetic field at the muon site. When oscillations are not resolvable, only the first term in Eq. 1) is measured, giving a signal whose amplitude is due to that component of the muon spin initially oriented parallel to the local magnetic field at the muon site. The re-

laxation of such a signal is due to the dynamic fluctuations of the local field at the muon site. In the fast magnetic fluctuation regime (typical of most magnetic materials) dynamics give rise to exponential relaxation³² $A(t) = A_0 \exp(-t) \cos^2 \theta$ with a relaxation rate given by $\Gamma = 2 \langle H^2 \rangle$, where $\langle H^2 \rangle$ is the second moment of the magnetic field distribution at the muon sites and is the correlation time describing the dynamics of the local field distribution. Dynamic fluctuation in the paramagnetic phase may also be expected to give rise to exponential relaxation, although in that case there is no angle dependence and $A(t) = A_0 \exp(-t)$. The spectra measured at ISIS show this expected exponential relaxation at all measured temperatures ($15 < T < 300$ K). The measured asymmetry for these data is best described by a fitting function

$$A(t) = A_1 e^{-t} + A_{\text{bg}}; \quad (2)$$

where A_{bg} represents the contribution from those muons that stop in the sample holder or cryostat tail. Note that the background signal due to muons stopping in PTFE is the distinctive $F\{+F\}$ state³⁴, so can be easily identified and subtracted.

Although it might be hoped that the temperature evolution of $A(t=0) = A_1$ in Eq. (2) would tell us the orientation of the local magnetic field at the muon site via Eq. (1), this is not the case here. This quantity (Fig. 2(a)) shows a decrease in the paramagnetic regime as temperature is reduced towards T_N . This points to the presence of an additional fast relaxation component that we do not resolve. The presence of two relaxation rates signals either two classes of muon site or to two relaxation channels (see Ref. 35 for a discussion). The amplitude $A(t=0)$ then shows quite scattered behavior in the HTI phase before levelling off in the HTII phase. The presence of an additional relaxing component makes any determination of the local field direction in the crystal very difficult.

In contrast, the relaxation rate provides a good probe of the magnetic behavior in HoMnO_3 . On cooling from $T = 300$ K the rate (Fig. 2(b)) is seen to increase with decreasing temperature, peaking around 79 K. This reflects the slowing of fluctuations of the $M^{\text{R}+}$ moments as the material approaches the magnetic phase transition at T_N where these moments magnetically order. On cooling further we observe that with decreasing temperature shows a weak, approximately linear, increase. Subtracting this trend from the data results in two pronounced minima, shown in Fig. 2(c), which occur at the two proposed transition temperatures between the phases HTI, IP and HTII. Fitting Lorentzian lineshapes to these features allows us to estimate the transition temperatures as $T_{\text{IP}} = 38.2(2)$ K and $T_{\text{HTII}} = 33.4(3)$ K. We note from our previous analysis that minima in Γ near the phase boundaries at T_{IP} and T_{HTII} would imply that $\langle H^2 \rangle$ goes through minima at these temperatures. This would correspond to correlation times which are shortest at these phase boundaries.

We note here that the largest change in Γ is seen at

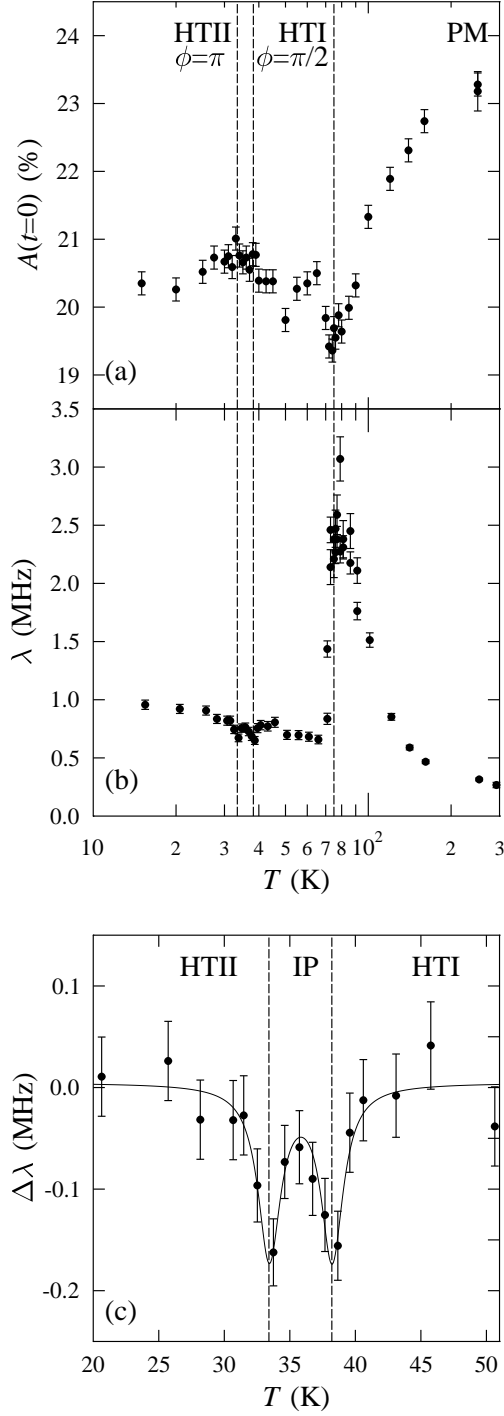


FIG. 2: Results for measurements made in ZF across the phase diagram. (a) Temperature dependence of the initial asymmetry $A(t=0)$. (b) Evolution of the relaxation rate with temperature. (c) Detail from (b) after background subtraction showing the behavior of λ at low temperature. Minima are observed at the phase boundary between HTI and IP phases and at that between IP and HTII phases.

$T = 79$ K where the Mn^{3+} spins first order and at which the Ho^{3+} spins have do not undergo any change. This contrasts with the changes seen below 38 K, where the Ho^{3+} spins begin to order, which are far more modest. This implies that, in our measurements, we are mostly sensitive to the fields due to the local magnetic fields due to the Mn spins. This is consistent with the case of structurally similar $YMnO_3$ ¹⁹, where ZF ^{51}V SR measurements revealed the existence of two separate classes of muon site, showing quite differently behaving relaxation rates. In $YMnO_3$, one site appeared to be closely coupled to the magnetic layers of Mn^{3+} ions, while the other was less well defined, but was probably due to sites between the layers. We might expect the muon sites in $HoMnO_3$ to be similar, with the site near the Mn layers giving rise to the relaxation with rate λ and the site between layers, coupled more strongly to the Ho^{3+} moments. This latter site would then be responsible for rapid relaxation in the PM phase which leads to the loss of initial asymmetry described above.

B. E-field + SR

E-field + SR measurements were made in the presence of a longitudinal magnetic field (LF) B_a directed along the crystal's c-axis. Static electric fields of $E = 10^4$ Vm⁻¹ were applied in the same direction. The saturation field of $HoMnO_3$ occurs at $E = 10^4$ Vm⁻¹, above which we expect a single ferroelectric domain.

As in the ZF case, the spectra for E-field + SR measurements showed exponential relaxation described by relaxation rate λ . Fig. 3 (a) and (c) show the results of applying a magnetic field B_a in the presence and absence of a static electric field E in the HTII phase (at $T = 30$ K) and the HTI phase (at $T = 50$ K). In both phases there is little systematic variation of λ as a function of applied magnetic field B_a , independent of the presence (or absence) of the E-field. It is expected that a dynamic relaxation rate should vary with applied magnetic field as $\lambda = 2^2 \hbar B_a^2 i = (\hbar^2 B_a^2 + 1)$; which suggests that we are in the limit that $\hbar^2 B_a^2 \gg 1$, or, given that the maximum field was 300 mT, $\hbar \approx 5$ ns. The main result of these measurements is that, in both HTI and HTII phases, the presence of the electric field E results in a reduction of the relaxation rate (λ) compared to ($E = 0$) of 0.5 MHz. Application of the paired-sample t-test shows that the E-field causes a statistically significant decrease at a $> 99\%$ confidence level in both phases. Fig. 3 (b) and (d) show the normalized difference in the relaxation rates with the field on and off, (i.e. $[\lambda(E=0) - \lambda(E)] / [\lambda(E=0)]$) as a function of B_a . Taking the average of these results across the B -field range shows the same average decrease in this quantity of 11 (1)% for each phase.

In interpreting these E-field dependent data we note first that the effect of applied E-field is the same within experimental uncertainties in the HTI and HTII phases.

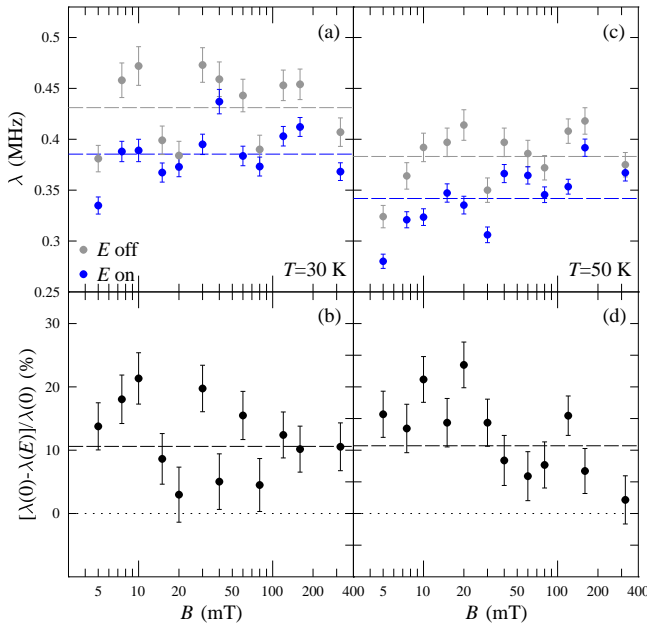


FIG. 3: (a) Relaxation rate λ at $T = 30$ K (HTII phase) in the presence and absence of an electric field. The average value for each condition is shown as a dashed line. The field is seen to reduce the mean value of λ . (b) Fractional difference in λ defined as $[\lambda(E=0) - \lambda(E)] / \lambda(E=0)$. The average difference is around 10% (dashed lines). (c) and (d) same as (a) and (b) but measured at $T = 50$ K (HTI phase).

This is in keeping with the optics results⁶ where the ME effect was seen at all temperatures below T_N and would imply that the change in Ho ordering at T_{SR} is not a prerequisite for the observation of a ME effect. Noting that in the fast fluctuation limit the relaxation rate $\propto \hbar B^2$, it is likely that the decrease in λ caused by the application of the E-field reflects a decrease in the quantity $\hbar B^2$, the local magnetic field distribution at the muon sites. (It seems unlikely that the E-field would cause a decrease in the correlation time.) There are two ways to decrease $\hbar B^2$: (i) a reduction in the magnitude of the average local magnetic field at the muon sites, caused, for example, by the E-field altering the magnetic moment structure via the magnetoelectric effect in such a way that the average dipole field at the muon sites decreases; (ii) a decrease in the width of the magnetic field distribution. For the case (ii) the E-field leads to an effective increase in the order in the magnetic structure. This, we believe, provides the most likely mechanism for our measurements.

The primary effect of applying a large E-field to a FE is to produce a single ferroelectric domain. Furthermore, it has been demonstrated experimentally in the case of YMnO_3 ³ (and proposed for HoMnO_3 ²⁶) that FE domain walls coincide with AFM domain walls. This may be explained by supposing that the lattice strain, which is present by virtue of the existence of the FE domain wall, couples to local magnetic moments. This means that the free energy of the system is lowered when the magnetic order parameter (i.e. the sublattice magnetic moment in an AFM) changes sign across a FE domain wall, creating a spatially coincident AFM wall. This implies that all FE domain walls coincide with AFM domain walls, but that AFM domain walls may exist within a single FE domain. The application of the E-field therefore causes not only a single FE domain, but also a reduction in the number of AFM domains. This will reduce the width of the magnetic field distribution $\propto \sqrt{B^2}$ probed by the muons and causes the small observed decrease in the relaxation rate. Our E-field + SR results may therefore be consistent with the magnetoelectric coupling in HoMnO_3 being mediated via domain walls, as was originally proposed to explain the results of dielectric constant measurements²⁶.

V. CONCLUSION

In conclusion, we have studied the ZF and E-field + SR of HoMnO_3 . We are able to confirm the presence of magnetic transitions at $T = 76$ K, $T = 34$ K and $T = 38$ K. The muon probe is primarily sensitive to the ordering and dynamics of the Mn^{3+} magnetic moments, with the Ho ordering having little effect on our measurements. The ordering of the Ho moments, at most, contributes via a minority relaxation channel. The application of electric fields of $E = 10^6$ Vm⁻¹ causes only a $\sim 10\%$ change in the relaxation rate, which may be accounted for by a reduction in the number of coupled FE and AFM domain walls.

Acknowledgments

Part of this work was carried out at the ISIS Facility, Rutherford Appleton Laboratory, UK and at the Swiss Muon Source, Paul Scherrer Institute, Villigen, Switzerland. We thank A. Amato for technical assistance and W. Hayes for useful discussions. This work is supported by the EPSRC.

¹ S.-W. Cheong and M. M. Mostovoy, *Nature Mater.* **6**, 13 (2007).

² N. A. Hill, *J. Phys. Chem. B* **104**, 6694 (2000).

³ M. Fiebig, Th. Lottermoser, D. Fröhlich, A. V. Goltsev, and R. V. Pisarev, *Nature (London)* **419**, 818 (2002).

⁴ T. Kimura, T. Goto, H. Shintani, K. Ishizaka, T. Arima,

- and Y. Tokura, *Nature (London)* 426, 55 (2003).
- ⁵ N. Hur, S. Park, P. A. Sharma, J. S. Ahn, S. Guha, and S.-W. Cheong, *Nature (London)* 429, 392 (2004).
 - ⁶ T. Lottermoser, T. Lonkai, U. Amann, D. Hohlwein, J. Thiringer, and M. Fiebig, *Nature (London)* 430, 541 (2004).
 - ⁷ M. Fiebig, *J. Phys. D* 38, R123 (2005).
 - ⁸ R. Ramesh and N. A. Spaldin, *Nature Mater.* 6, 21 (2007).
 - ⁹ B. B. Van Aken, T. T. M. Palstra, A. Filippetti, and N. A. Spaldin, *Nature Mater.* 3, 164 (2004).
 - ¹⁰ B. Lorenz, A. P. Litvinchuk, M. M. Gospodinov, and C. W. Chu, *Phys. Rev. Lett.* 92, 087204 (2004).
 - ¹¹ N. Hur, I. K. Jeong, M. F. Hundley, S. B. Kim, and S.-W. Cheong, *Phys. Rev. B* 79, 134120 (2009).
 - ¹² O. P. Vajk, M. Kenzelmann, J. W. Lynn, S. B. Kim, and S.-W. Cheong, *Phys. Rev. Lett.* 94, 087601 (2005).
 - ¹³ F. Yen, C. R. dela Cruz, B. Lorenz, Y. Y. Sun, Y. Q. Wang, M. M. Gospodinov, and C. W. Chu, *Phys. Rev. B* 71, 180407(R) (2005).
 - ¹⁴ C. dela Cruz, F. Yen, B. Lorenz, Y. Q. Wang, Y. Y. Sun, M. M. Gospodinov, and C. W. Chu, *Phys. Rev. B* 71, 060407(R) (2005).
 - ¹⁵ H. Lueken, *Angew. Chem. Int. Ed.* 120, 8690 (2008).
 - ¹⁶ G. A. Gehring, *Ferroelectrics* 161, 275 (1994).
 - ¹⁷ T. Lottermoser and M. Fiebig, *Phys. Rev. B* 70, 220407(R) (2004).
 - ¹⁸ F. Bert et al., *Phys. Rev. Lett.*, 97 117203 (2006); P. Dalmas de Reotier, et al. *Phys. Rev. Lett.* 96, 127202 (2006); X. G. Zheng, et al. *Phys. Rev. Lett.* 95, 057201, (2005).
 - ¹⁹ T. Lancaster, S. J. Blundell, D. Andreica, M. Janoschek, B. Roessli, S. N. Gvasaliya, K. Conder, E. Pomjakushina, M. L. Brooks, P. J. Baker, D. Prabhakaran, W. Hayes and F. L. Pratt, *Phys. Rev. Lett.* 98, 197203, (2007).
 - ²⁰ D. G. Eshchenko, V. G. Storchak, G. D. Morris, *Phys. Lett. A* 264, 226 (1999).
 - ²¹ V. G. Storchak, O. E. Parfenov, J. H. Brewer, P. L. Russo, S. L. Stubbs, R. L. Lichti, D. G. Eshchenko, E. M. Morenzoni, V. P. Zolotarev, A. A. Vinokurov and V. G. Baburov, *Physica B* 404, 899 (2009).
 - ²² F. Yen, C. dela Cruz, B. Lorenz, E. Gastylan, Y. Y. Sun, M. Gospodinov and C. W. Chu, *J. Mater. Res.* 22, 2163 (2007).
 - ²³ A. Munoz, J. A. Alonso, M. J. Martinez-Lope, M. T. Casais, J. L. Martinez and M. T. Fernandez-Diaz, *Chem. Mater.* 13, 1497, (2001).
 - ²⁴ T. Lonkai, D. Hohlwein, J. Thiringer, and W. Prandl, *Appl. Phys. A: Mater. Sci. Process.* 74, S843 (2002).
 - ²⁵ S. Nandi, A. Kreyssig, L. Tan, J. W. Kim, J. Q. Yan, J. C. Lang, D. Haskel, R. J. McQueeney and A. I. Goldman, *Phys. Rev. Lett.* 100, 217201 (2008).
 - ²⁶ B. Lorenz, A. P. Litvinchuk, M. M. Gospodinov and C. W. Chu, *Phys. Rev. Lett.* 92, 087204 (2004).
 - ²⁷ P. Coeure, F. Guinet, J. C. Peuzin, G. Buisson and E. F. Bertaut in *Proc. of 1st Intl. Meeting on Ferroelectricity (Institute of Physics, Czech. Acad. Sci., Prague, 1996)*, p.332.
 - ²⁸ H. D. Zhou, J. C. Denyszyn and J. B. Goodenough *Phys. Rev. B* 72, 224401 (2005).
 - ²⁹ S. J. Blundell, *Contemp. Phys.* 40, 175 (1999).
 - ³⁰ S. G. Barsov, S. I. Vorob'ev, V. P. Koptev, E. N. Komarov, S. A. Kotov, S. M. Mikitych'yants, G. V. Shcherbakov, A. E. Pestun and Ya. M. Mukovskii, *JETP* 85, 658 (2007).
 - ³¹ E. Gastylan, B. Lorenz, K. S. Martirosyan, F. Yen, Y. Y. Sun, M. M. Gospodinov and C. W. Chu, *J. Phys. Condens. Matter* 20, 325241 (2008).
 - ³² R. S. Hayano, Y. J. Uemura, J. Imazato, N. Nishida, T. Yamazaki and R. Kubo, *Phys. Rev. B* 20, 850 (1979).
 - ³³ R. Pauthenet and C. Veyret, *J. Phys.*, 31 65 (1970).
 - ³⁴ T. Lancaster, F. L. Pratt, S. J. Blundell I. McKenzie and H. E. Assender, *J. Phys. Condens. Matter*, 21 346004 (2009).
 - ³⁵ T. Lancaster, S. J. Blundell, P. J. Baker, H. J. Lewtas, W. Hayes, F. L. Pratt, H. T. Yi and S.-W. Cheong, *Phys. Rev. B*, 80, 020409(R) (2009).